

The influence of air inlet layout on the inner flow field for a vertical turbo air classifier

Yuan Yu ¹, Xingshuai Li ¹, Yu Zhang ¹, Zhiwei Jiao ¹, Jiaxiang Liu ²

¹ College of Mechanical and Electrical Engineering, Beijing University of Chemical Technology, Beijing 100029

² College of Materials Science and Engineering, Beijing University of Chemical Technology, Beijing 100029

Corresponding authors: tougao_20192019@163.com (Yuan Yu), ljxpost@263.net (Jiaxiang Liu)

Abstract: In this study, the influence of air inlet layout on the flow field distribution and particle movement trajectory for the vertical turbo air classifier are analyzed comparatively using the numerical simulation method. The air inlet layout adjustment can increase the axial velocity and turbulent dissipation rate at the feeding inlet and do not generate the axial negative velocity, which improves powder material pneumatic transportation and dispersion capacity; the air inlet layout adjustment can match the airflow rotation direction with the rotation direction of the rotor cage, which can eliminate the vortices in the rotor cage channel effectively. Moreover, the particle movement time is shortened and fast classification is completed, which can decrease the particle agglomeration probability and weaken the 'fish-hook' effect. The optimization scheme of the air inlet layout is Type-BC. In accordance with the numerical simulation results, the calcium carbonate classification experimental results indicate that the classification performance of the classifier is improved using Type-BC.

Keywords: turbo air classifier, powder technology, air inlet layout, numerical simulation, classification performance

1. Introduction

The process of crushing, grinding, and classification to obtain ultrafine powder is a physical preparation method with the features of low cost, large outputs, and simple preparation, which is widely used in industry. Based on the centrifugal force field, the heterogeneous system can be separated effectively. It means there are different forces acting on the coarse and fine particles in the moving airflow. Thus, the different movement trajectories of the particles and the classification of the coarse and fine particles can be realized. With the strict requirements of particle size distribution, increasing the powder product fineness and single machine outputs, and the demand of decreasing of the energy consumption, the pneumatic classification has become the key technology of preparation of ultrafine powder by mechanical method. For a long time, several scholars have improved and innovated the structures of pneumatic classifiers (Huang et al., 2012; Ren et al., 2016; Guizani et al., 2017; Petit and Irassar, 2021; Kaas et al., 2022).

Air inlet layout is an important factor in the design of separators including cyclone separators and pneumatic classifiers, which determines the direction and velocity of airflow and distribution characteristics of the flow field in the separators. Reasonable air inlet layout can effectively improve the flow field distribution and material classification effect (Su et al., 2011; Winfield et al., 2013). Marek and Lakhbl (2019) studied the effects of the inlet angle of cyclone separators on the flow field. The results showed that air inlet angle influenced the classification efficiency. The classification efficiency was the highest when the vertical direction was 90° and it was the lowest when the vertical direction was -45°. Lim et al. (2020) installed additional inlets on the cone section of the conventional tangential cyclone separator. The optimized cyclone separator processed a higher flowrate of aerosol than that of the original separator with a similar classification efficiency and pressure drop. Mageshwaran et al. (2018) compared the flow field characteristics of cyclone separators with single and double air inlet structures. It was found that the separator with a double air inlet had a well-distributed pressure field and a high

separation efficiency. Gao et al. (2020) compared cyclone separators with different air inlet layouts and found that proper adjustment of air inlet layout could balance vortex structure in separators and improve separation efficiency. Sun et al. (2019) modified the traditional tangential air inlet into the radial air inlet, and altered the air inlet into the type of louver to obtain the well-distributed flow field and improve the classification performance of the classifier. Additionally, Sun et al. (2021) improved the air inlet method of the horizontal turbo air classifier: the material was fed to the classification region with the tangential primary wind to increase the dispersion of the material, and the secondary wind entered from the low elutriation area to significantly improve the classification accuracy. Feng et al. (2020) obtained the swirling inlet and the non-swirling inlet by changing the incidence angle of the inlet nozzle and they measured the flow field adjacent to the rotor cage blade using the Particle Image Velocimetry (PIV) technique. The results showed that the separation efficiency of the classifier with the swirling inlet was higher than that of the classifier with the non-swirling inlet.

In conclusion, many researchers have improved the classification performance of the equipment by optimizing the air inlet structure or adjusting the air inlet layout according to the structural characteristics of the different types of pneumatic separators. The vertical turbo air classifier is widely used in the chemical industry, construction industry, metallurgy, paper industry, pharmaceutical enterprise, and other fields. However, the influence of the air inlet layout of the classifier on the flow field and classification effect as well as the optimization of the inlet layout of the turbo air classifier have rarely been reported. In this study, the flow field in the vertical turbo air classifier is simulated using the Computational Fluid Mechanics (CFD) Software ANSYS. The characteristics of different air inlet layout schemes are compared from the perspectives of the transportation capacity of airflow for powder materials, the uniformity of flow field distribution, and the vortices distribution in the rotor cage channels between blades. According to the material experiments, the optimized scheme for the air inlet layout of a vertical turbo air classifier is proposed, which provides theoretical guidance for the design and manufacture of the pneumatic classifier.

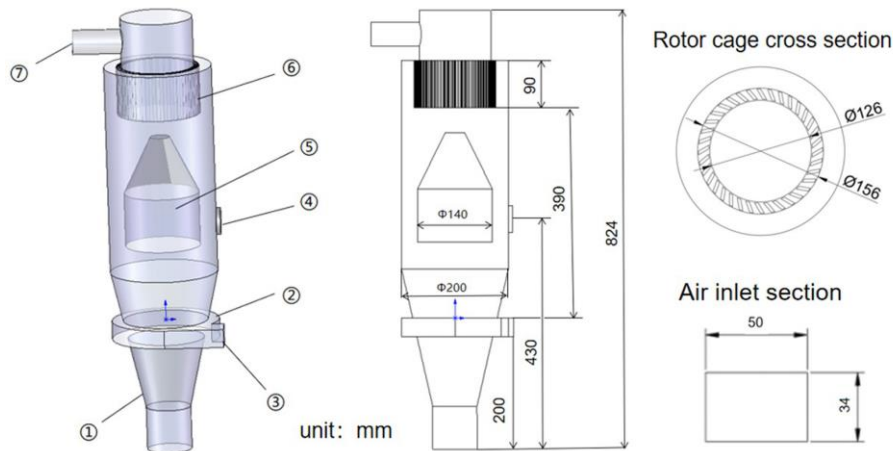
2. Model of a vertical turbo air classifier

2.1. Working principle of the equipment

A schematic illustration of the vertical turbo air classifier is shown in Fig. 1 and the working principle is as follows: Under the suction action of the fan, the air enters the air intake volute ② tangentially through the air inlet ③ in the air intake region and forms a rotating airflow. The airflow rotates and rises to the main classification region (the annular region between the outer edge of the rotor cage and the cylinder wall of the classifier) passing by the spoiler cone ⑤ in the elutriation region. After crossing the central region of the rotor cage ⑥ (the rotor cage is driven by the motor shaft and it rotates clockwise around Z axis), the airflow leaves the classifier through the fine powder outlet ⑦. The powder is fed into the elutriation region from the feeding inlet ④ through the spiral feeding device for 'pre-dispersion', and the particles are transported to the annular region with the rotating rising airflow, where the coarse and fine particles are mainly separated. After the main classification process, the fine particles flow out from the fine powder outlet via the rotor cage channel with the airflow and then they are collected as fine powder. The coarse particles lose kinetic energy after colliding with the cylinder wall and fall into the coarse powder collection funnel ① along the side wall of the cylinder under the action of gravity, finally are collected as coarse powder.

The model of the turbo air classifier is established using Solidworks software. The turbo air classifier is 824 mm high and the outer diameter of the cylinder is 200 mm; the coarse powder collection funnel is 200 mm high; the cross-section of the air inlet is 50 mm wide and 34 mm high; the air intake volute has a diameter of 200 mm and a height of 40 mm. The air inlet and the air intake volute are installed tangentially. The upper region of the air intake volute to the lower region of the rotor cage is the elutriation region with a height of 390 mm. A spoiler cone with a diameter of 140 mm is installed in the elutriation region, which is coaxial with the cylinder body. The center of the bottom surface of the spoiler cone is the origin of the model, and this plane is $Z=0$ mm. The feeding inlet is 430 mm high and 50 mm in diameter, which is vertically installed with the axis line of the classifier. There is an annular region between the outer edge of the rotor cage and the cylinder body, and the annular region is 90 mm high. The rotor cage has an inner diameter of 126 mm, an outer diameter of 156 mm, and a height of 90 mm.

36 blades of the rotor cage are distributed uniformly along the circumference of a circle with a diameter of 141 mm and oriented at an angle of 120 degrees from the tangent at the point on the circle coincident with the blade's centroid. The length of the rotor cage blade is 15 mm, its width is 5 mm, and its height is 90 mm. The rotor cage center and the fine powder outlet are the central region, with a height of 200 mm.



① Coarse powder collection funnel ② Air intake volute ③ Air inlet ④ Feeding inlet
⑤ Spoiler cone ⑥ Rotor cage ⑦ Fine powder outlet

Fig. 1. Schematic illustration of the vertical turbo air classifier

2.2. Description of simulation conditions

The software ICEM is used to generate meshes for the vertical turbo air classifier model, shown in Fig. 2. The classifier is divided into five regions: coarse powder collection region, air intake region, elutriation region, rotor cage region, and central region.

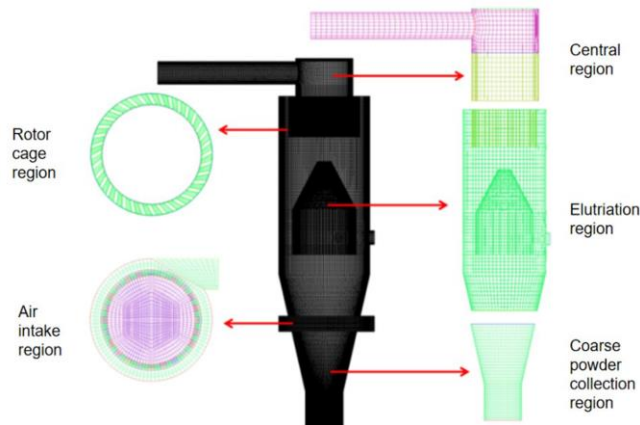


Fig. 2. The meshes of the vertical turbo air classifier

The hexahedral meshes have the advantages of high mesh quality, accurate calculation, and suitable mesh quantity under the same volume compared to the other meshes, which are used in this classifier model. The mesh independence verifications are conducted and 4.63 million meshes for the model are determined before the numerical simulation (Wang et al., 2021). The flow field in the turbo air classifier is numerically simulated using ANSYS Software, in which the rotor cage region is moving and the rest regions are static. Their interaction is settled using Multiple Reference Frame (MRF). The MRF model is a steady-state approximation in which different rotation and translation speeds can be assigned to each mesh unit, and each moving mesh zone is solved by the moving reference frame equations. Yu et al. (2022) compared the steady-state and transient-state calculations using the MRF model. The results showed that after the iteration converged, the flow fields under the steady-state conditions in the annular region and rotor cage channel were consistent with those calculated under the transient-state

conditions even with different time steps. The reason is that the operating parameters of the turbo air classifier including air inlet velocity, rotor cage rotating speed, and feeding speed remain unchanged during the stable working conditions, and the main physical parameters of the flow field including speed and pressure are almost constant. Therefore, the flow field is stable and the steady-state approximate solution of the flow field can be carried out. The RNG k- ϵ two-equation model is suitable for the simulation of swirling flow, high strain rate and flow line curvature (Ren et al., 2016; Martin et al., 2017), so it is selected for this application. The SIMPLEC algorithm is applied for the coupling of pressure and velocity. The convergence residual is set to $10e-4$. The inlet boundary condition is set as 'velocity-inlet' and the outlet boundary condition is set as 'outflow'. For ease of expression, air inlet velocity (m/s) - rotor cage speed (rpm) is adopted to represent the combination of operating parameters. For example, the operating condition is 29-800, which means the air inlet velocity is 29 m/s and the rotor cage speed is 800 rpm.

Pressure drop is one of the important measurement indices of the air classifier, which is often used to verify the accuracy of simulation results (Hagemeier et al., 2014; Sun et al., 2017). In this study, under 29-800 and 29-1600 operating conditions, the experimental and simulated pressure drops of single-phase airflow are compared to verify the reliability of this numerical model. The simulated pressure drop is the difference between the area-weighted average static pressure of the air inlet and that of the air outlet. The experimental pressure drop is the difference between the pressures of the air inlet and the air outlet measured by the U-type differential pressure meter (CJM-580 model, Hengshui Chuangji Instrument Co., LTD.). The results are shown in Table 1. The relative deviations of the pressure drop between the air inlet and the air outlet are 1.3% and 2.4%, respectively. Therefore, the simulation results obtained under the above simulation conditions are reliable.

Table 1. Comparison of experiment and simulated pressure drops between the air inlet and outlet

Operating Conditions	29-800	29-1600
Experimental value (Pa)	2160	2250
Simulated value (Pa)	2131	2196
Deviation (%)	1.3%	2.4%

2.3. Design of the air inlet layout schemes

The laboratory-scaled prototype of the vertical turbo air classifier shown in Fig.1, and the feeding inlet and the air inlet are located on the same side of the classifier. The center of the feeding inlet passes through the axis line of the classifier, and the air inlet is tangential to the air intake volute from the left side of the air intake region, and the airflow enters the classifier from the air inlet and forms a counter-clockwise swirl. For the convenience of expression, the air inlet layout scheme of this prototype is named as Type-Proto. To enhance pneumatic transportation for powder material in the elutriation region, the air inlet of Type-B is mirrored to Type-Proto and it has a position difference of 180° compared with Type-Proto, shown in Fig.3. In Type-B, the airflow maintains a counter-clockwise swirling flow in the classifier.

The airflow in the annular region moves as a free vortex and then moves as a forced vortex driven by the rotor cage rotation after entering the rotor cage. When the airflow enters the rotor cage, it impacts the blade at a certain angle, which is called impact angle δ . The difference between the airflow relative velocity angle β (the angle between the vectors of the relative velocity and the implicated velocity) and the blade installation angle θ (the angle between the blade and the implicated velocity). The larger the impact angle, the stronger the impact of airflow on the blade is, and the more unstable the flow field is. Thus, the vortex is formed (Tang et al., 2013). In order to obtain the well-distributed flow field in the rotor cage channels of the classifier and eliminate the vortices, Type-C is proposed to reduce the impact angle of airflow on the blades when the airflow enters the rotor cage. The air inlet of Type-C is on the same side as the feeding inlet. Compared with the Type-Proto and Type-B, the air inlet of Type-C is tangential to the intake volute and makes the airflow forming a clockwise swirling flow after entering the classifier, shown in Fig. 3.

To improve the flow field in the elutriation region for powder materials pneumatic transportation capability and increase the uniformity of flow field distribution in the rotor cage channel and eliminate the vortices between blades, Type-BC is designed to further optimize the air inlet layout of the classifier combining Type-B and Type-C. The air inlet of Type-BC is mirrored from Type-C. The airflow rotation of Type-BC is the same as that of the Type-C, which is clockwise, shown in Fig. 3.

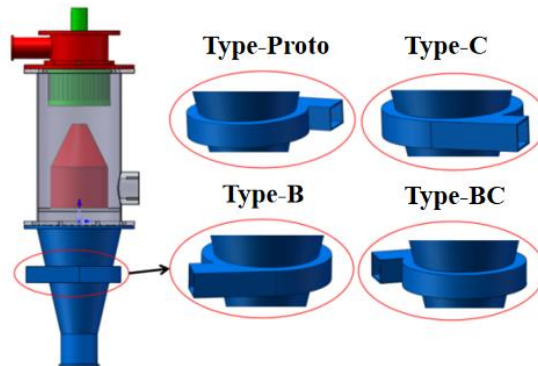


Fig. 3. Schematic illustration of four air inlet layout schemes

3. Results and analyses

3.1. Flow field in elutriation region of the turbo air classifiers

In the flow field of a vertical turbo air classifier, the airflow enters the classifier tangentially from the air inlet and spirals upward, the streamlines of the classifiers with four different air inlet layout schemes are shown in Fig. 4. For Type-Proto and Type-C, the airflow spirals upward far from the feeding inlet; For Type-B and Type-BC, the airflow trajectory presents a position difference of 180° and the airflow spirals upward near the feeding inlet compared with Type-Proto and Type-C. Figure. 5 shows the axial velocity contour on the XOZ plane of the elutriation region of the four classifiers. It can be observed obviously that the axial velocity contours of the elutriation region for Type-Proto and Type-C are almost same, shown in Fig. 5(a) and (c). The axial velocity value of the elutriation region ranges from -6.7 m/s to 13.6 m/s, where the negative axial velocity indicates that its direction is vertically downward. It shows that there exist negative axial velocities at many places, with a large value near the feeding inlet. Under the action of negative axial velocity, part of the raw material fed into the classifier through the feeding inlet falls directly to the coarse powder collection region, resulting in the increase of the fine particles in the coarse powder, which will decrease the classification accuracy and aggravate the 'fish-hook' effect. For Type-Proto and Type-C, the maximum positive axial velocity is far away from the feeding inlet, which is not conducive to transporting raw materials to the annular region. The positive axial velocity is one of the key factors for transporting raw materials to the annular region to classify coarse and fine particles. The axial velocity value of Type-B and Type-BC are almost same, shown in Fig. 5(b) and (d). The axial velocity contours of Type-B and Type-BC have little difference from those of Type-Proto and Type-C. However, the axial velocity distributions of Type-B Type-BC and those of Type-Proto and Type-C are mirrored. For Type-B and Type-BC, there are the maximum axial velocities at the feeding inlet, which are positive. The negative axial velocities are far away from the feeding inlet. After entering the classifier from the feeding inlet, the raw materials are carried to the annular region by the upward airflow passing by the elutriation. Compared with Type-Proto and Type-C, Type-B and Type-BC can improve the powder material pneumatic transportation effectively.

The turbulent dissipation rate ε indicates small-size eddies with high-frequency pulsation. The larger the turbulent dissipation rate, the more eddies are. These small-size eddies are conducive to disaggregation. Figure 6 shows the turbulent dissipation rates concours on the XOZ plane of the classifiers with four different air inlet layout schemes. It can be seen that there is little difference in the values of turbulent dissipation rates of the four schemes, but the distributions of Type-Proto and Type-C are opposite to those of Type-B and Type-BC. For Type-Proto and Type-C, the high turbulent dissipation rates are far away from the feeding inlet; For Type-B and Type-BC, the high turbulent dissipation rates are near the feeding inlet. It shows that the small-size eddies with high-frequency

pulsation are distributed near the feeding inlet of Type-B and Type-BC, which will improve the pre-dispersion of raw materials effectively.

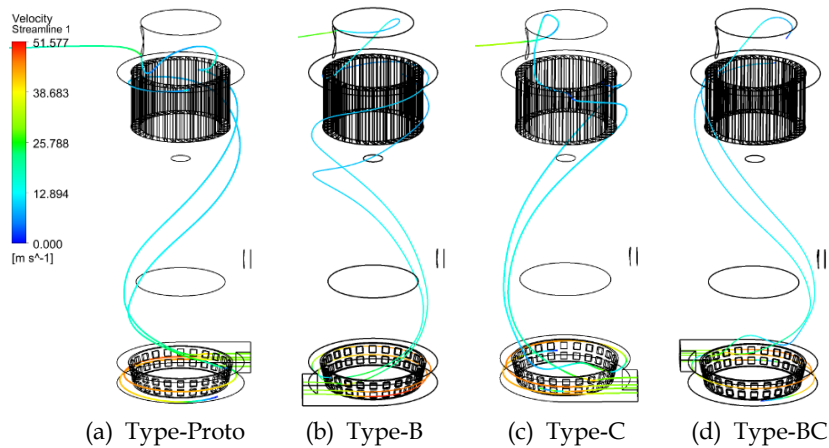


Fig. 4. Velocity streamline of the four classifiers

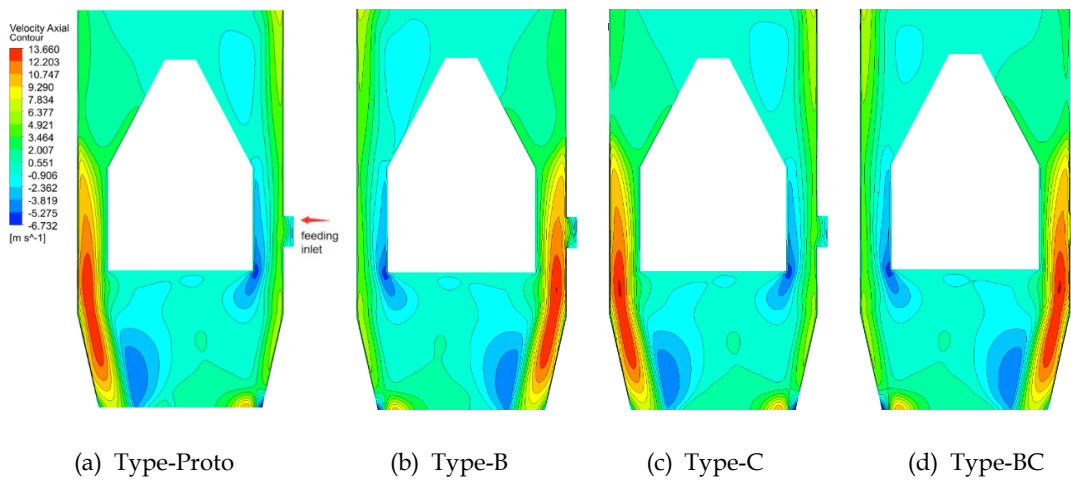


Fig. 5. Axial velocity contour on the XOZ plane of the elutriation region of the four classifiers

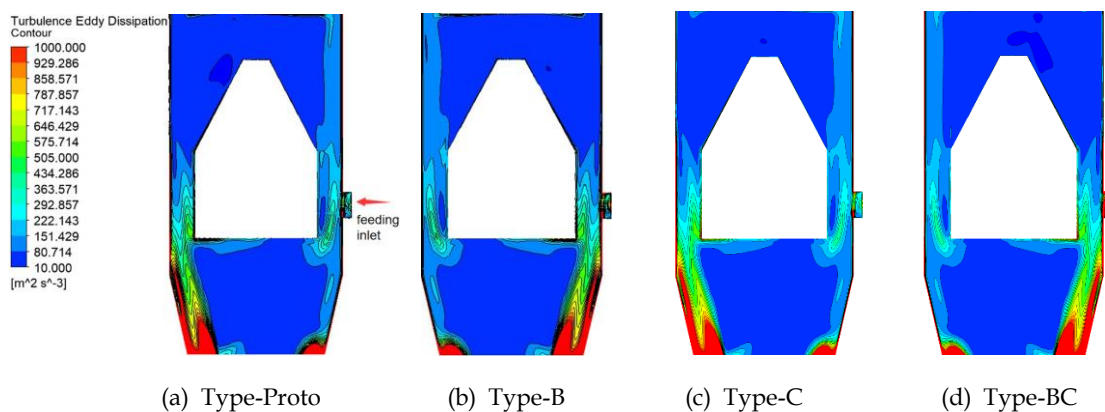


Fig. 6. Turbulence dissipation rate contours on the XOZ plane of the four classifiers

3.2. Flow field in rotor cage channels of the turbo air classifiers

In the annular region, when the air drag force acting on the particle is greater than the centrifugal force acting on the particle, the particle will enter the rotor cage channel, leave the center of the rotor cage with the airflow and then is collected as fine particle. Therefore, the flow field distribution in rotor cage

channels is one of the important factors influencing the classification performance. Figure 7 shows the radial velocity contours on the XOY plane ($Z=340$ mm) in the rotor cage channels of the classifiers with four different air inlet layout schemes. The negative radial velocity indicates that its direction points to the center of the rotor cage. The rotating direction of the rotor cage is clockwise. The rotating speed of the rotor cage is ω r/min. The flow field between the two blades selected is amplified to observe clearly. The radial velocity gradients of the flow fields are large in the rotor cage channels for Type-Proto and Type-B, shown in Fig.7 (a) and (b). The radial velocity of the airflow reaches -8.5 m/s near the pressure surface and 3.5 m/s near the suction surface. The large radial velocity gradient especially the vortex will cause the back-mixing of both coarse and fine particles. The fine particles that are dragged into the rotor cage channels will probably be returned to the annular region and mixed with the coarse powder by the airflow with the positive radial velocity (3.5 m/s) near the suction side of the rotor blade, which influences the classification effect (Ren, 2019). Obviously, for Type-C and Type-BC, the radial velocities of the airflow are negative, and there are no vortices in the rotor cage channels. The radial velocity distributions are well-distributed.

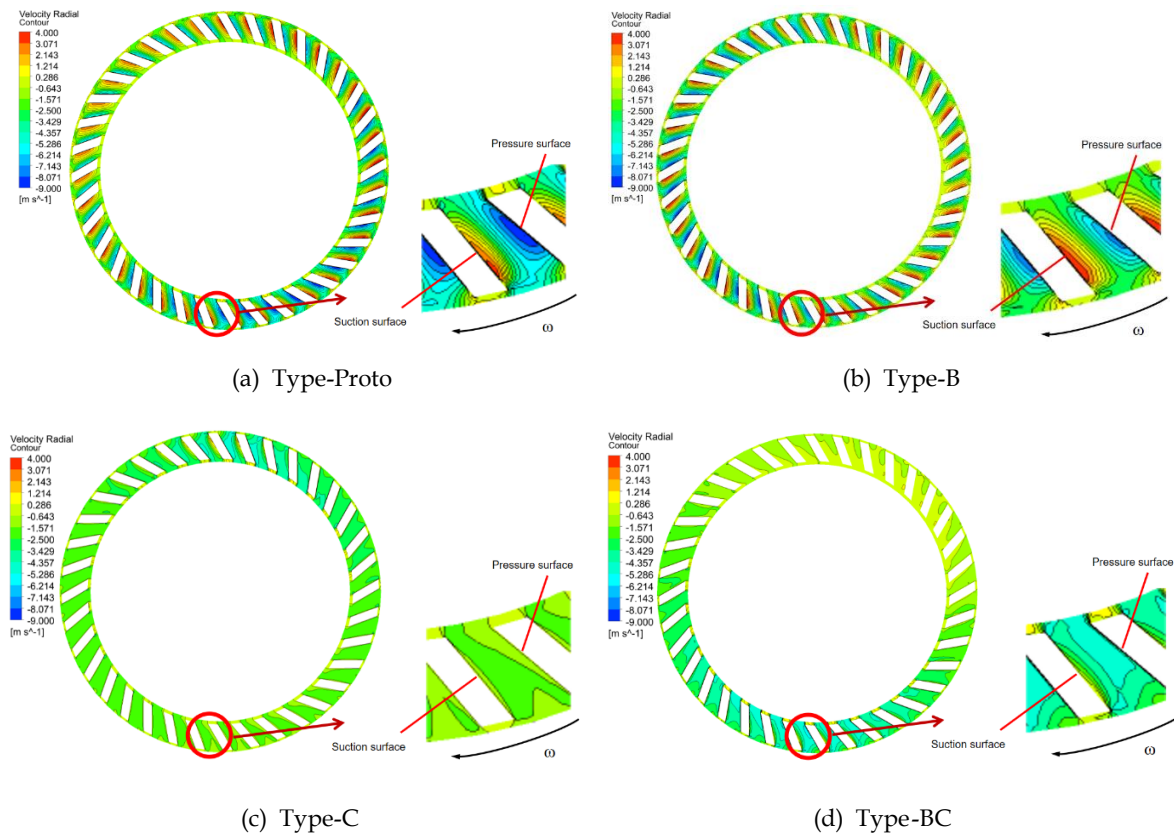


Fig. 7. Radial velocity contours in rotor cage channel of the four classifiers

The rotation of rotor cage will influence the flow field in the annular region. The flow field close to the rotor cage will be influenced strongly. The coarse and fine particles will be separated mainly at the interface of the rotor cage and the annular region (the outer edge of the rotor cage). For Type-Proto and Type-B, the rotation direction of the airflow is opposite to that of the rotor cage; however, for Type-C and Type-BC, the rotation direction of the airflow is the same as that of the rotor cage. Thus, the influences of the rotating rotor cage on the flow field in the annular region are different. In Fig. 7, the radial velocity distributions are well-distributed if the whirlwind direction is same as the rotating direction of the rotor cage. To further illustrate the reasons, the impact angles of airflow on the blades when the airflow enters the rotor cage are analyzed. To simplify the expression, Type-Proto and Type-C are taken as examples.

Under the design condition of 29-800, at the inlet of the rotor cage channels (the outer edge of the rotor cage and its diameter is 150 mm) of Type-Proto, the average radial velocity $V_{r1}=2.3$ m/s and the

average tangential velocity $V_{t1}=4.7$ m/s. The absolute velocity $V_1=5.2$ m/s and the absolute velocity angle (the angle between the absolute velocity and the implicated velocity) $\gamma_1=153.7^\circ$ can be calculated according to Eqs. 1 and 2, respectively. The velocity triangle at the inlet of the rotor cage is shown in Fig. 8(a).

$$V = \sqrt{V_r^2 + V_t^2} \quad (1)$$

$$\gamma = \begin{cases} \arctan \frac{V_r}{V_t}, & \text{if } V_t \text{ and } U \text{ are in the opposite direction} \\ 180 - \arctan \frac{V_r}{V_t}, & \text{if } V_t \text{ and } U \text{ are in the same direction} \end{cases} \quad (2)$$

The implicated velocity, U_1 , is the velocity of the outer edge of the rotor cage, and $U_1=6.3$ m/s can be calculated by Eq. 3.

$$U = \frac{\omega \pi R}{30} \quad (3)$$

where: ω_1 - rotor cage speed, r/min, R_1 - Radius of outer edge of cage, mm. The relative velocity and relative velocity angle are calculated by the law of cosines: $W_1=11.2$ m/s, $\beta_1=168.1^\circ$.

$$W = \sqrt{U^2 + V^2 - 2UV \cos \gamma} \quad (4)$$

$$\beta = 180 - \arccos \frac{U^2 + W^2 - V^2}{2UW} \quad (5)$$

The blade installation angle θ is 66° , and the impact angle δ_1 is 102.1° , which is the difference between the airflow relative velocity angle β and the blade installation angle θ . In Fig. 9, the vector length represents the magnitude of the relative velocity, and the arrow represents the direction of the relative velocity. It can be found that due to the large impact angle, the radial velocity gradient of the flow field in the rotor cage channel is large, resulting in an obvious vortex in the channel between blades, shown in Fig.9(a). In the same way, shown in Fig. 8 (b), under the same working conditions, for Type-C, $V_{r2}=1.8$ m/s, $V_{t2}=7.3$ m/s, $V_2=7.5$ m/s, $\gamma_2=13.9^\circ$, $U_2=6.3$ m/s, $W_2=2.0$ m/s, $\beta_2=61.4^\circ$, $\theta=66^\circ$ can be calculated. Thus, the impact angle δ_2 is 4.6° . Due to the small impact angle, there is no vortex in the rotor cage channels, shown in Fig. 9 (b).

In Fig.9, the airflow relative velocity at the outer edge of the rotor cage in Type-Proto ($W_1=11.2$ m/s) is larger than that of Type-C ($W_2=2.0$ m/s), and the relative velocity angle at the outer edge of the rotor cage in Type-Proto ($\beta_1=168.1^\circ$) is larger than that of Type-C ($\beta_2=61.4^\circ$). This is because the flow field in the annular region is influenced by rotation of the rotor cage. In Type-Proto, the rotation direction of the airflow is opposite to that of the rotor cage. When the airflow is close to the rotor cage, the rotor blades have a great resistance to the airflow. Thus, there are large relative velocity W and relative velocity angle β , shown in Fig. 9 (a). In Type-C, because the rotation direction of the airflow is the same as that of the rotor cage, the tangential velocity of the airflow is in the same direction as that of the rotor cage, and the rotor cage blades have little resistance to the airflow. Therefore, there are small relative velocity W and relative velocity angle β , shown in Fig. 9 (b).

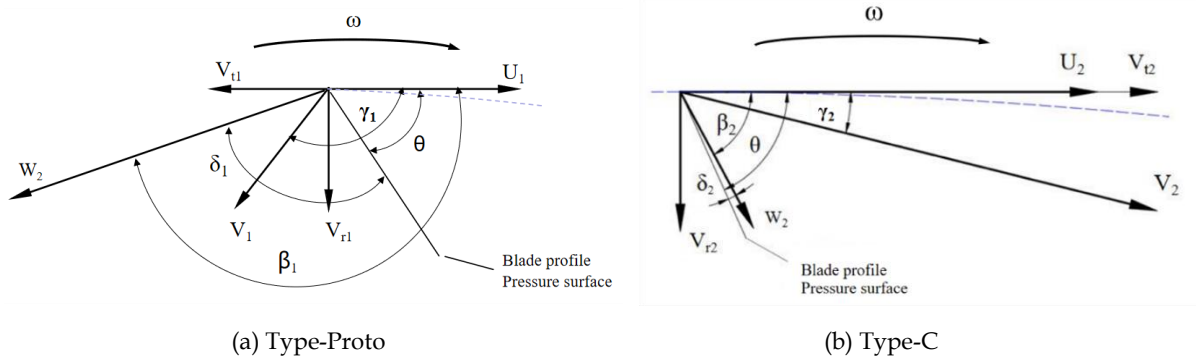


Fig. 8. The velocity vectors at the inlet of the rotor cage channel of Type-Proto and Type-C

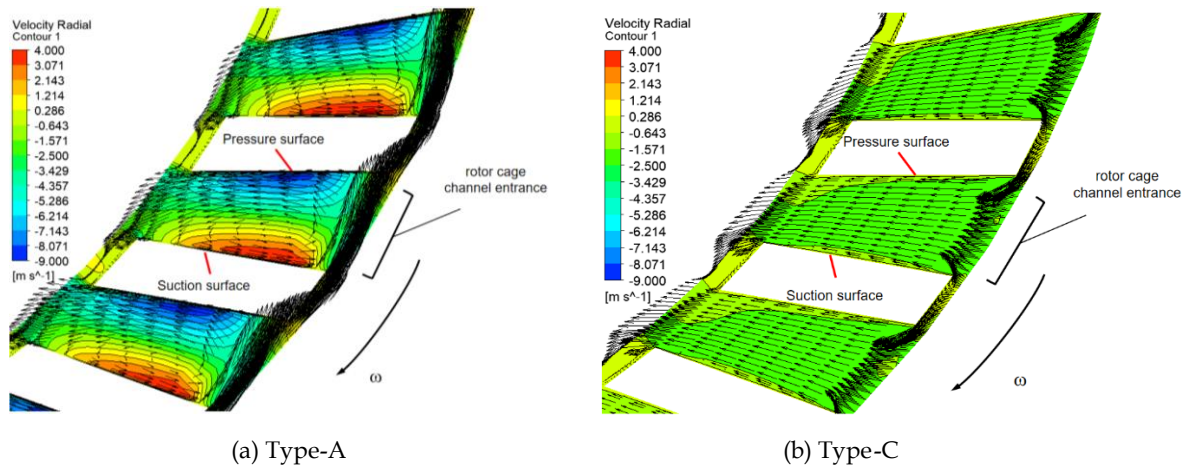


Fig. 9. Radial velocity contours and relative velocity vector in rotor cage channel of Type-Proto and Type-C

3.3. Comparative analysis of particle motion trajectory for the classifiers

According to Section 3.1, compared with Type-Proto and Type-C, Type-B and Type-BC improve the distribution of airflow axial velocity in the elutriation region, which is conducive to the transportation of the raw material. The Discrete Phase Model (DPM) is used and simulated the movement trajectory of particles in the elutriation region with the sizes from $10\ \mu\text{m}$ to $50\ \mu\text{m}$ in the classifier, shown in Fig. 10. For the Type-Proto and Type-C, some particles will continue to move upward with the airflow and reach the annular region for classification, while some particles will fall directly and be collected as coarse powder without separation. For Type-B and Type-BC, the particles with the sizes from $10\ \mu\text{m}$ to $50\ \mu\text{m}$ do not fall after entering the classifier but move upward with the airflow. Therefore, Type-B and Type-BC have better powder material pneumatic transportation capacity compared with those of Type-Proto and Type-C. This is because the axial velocities at the feeding inlets of Type-Proto and Type-C are small and there exist the negative velocities, while the axial velocities at the feeding inlets of Type-B and Type-BC are positive and the value are large.

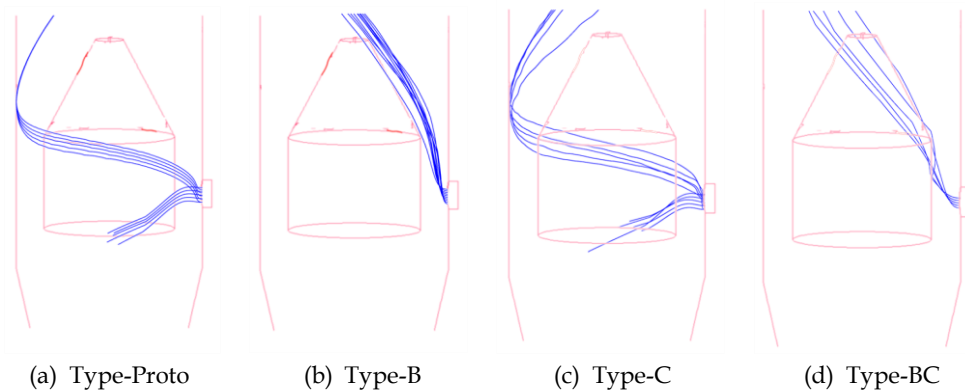


Fig. 10. Particle motion trajectories in the classifiers with different air inlet layout schemes

According to Section 3.2, compared with Type-Proto and Type-B, Type-C and Type-BC improve the flow field in the rotor cage channels to avoid obvious vortices. The single particle with the size of $10\ \mu\text{m}$ is released from the feeding inlet of the classifiers with four different air inlet layout schemes respectively and the motion trajectories are shown in Fig. 11. For Type-Proto and Type-B, the particles enter the rotor cage channel and then they are collected as a fine powder after they repeatedly hit the rotor cage blades for several times due to the vortices between blades. The movement time of particles in the classifier are 0.33 s and 0.29 s, respectively. The long movement time of the particle in the classifier will increase the probability of collision with other particles. It may be collected as coarse powder finally after its movement trajectory is changed. For Type-C and Type-BC, the flow field between the rotor cage

blades is well-distributed and there exists no vortices. The particle enters the rotor cage through the channel and is collected as a fine powder. The movement time of particles in the classifier are 0.26 s and 0.19 s, respectively. Since the flow field distribution in the elutriation region of Type-BC is more conducive to powder material pneumatic transportation, the movement time of this particle in Type-BC is shorter than that in Type-C. Rapid classification can reduce the probability of collision and agglomeration among ultrafine particles and improve the classification performance.

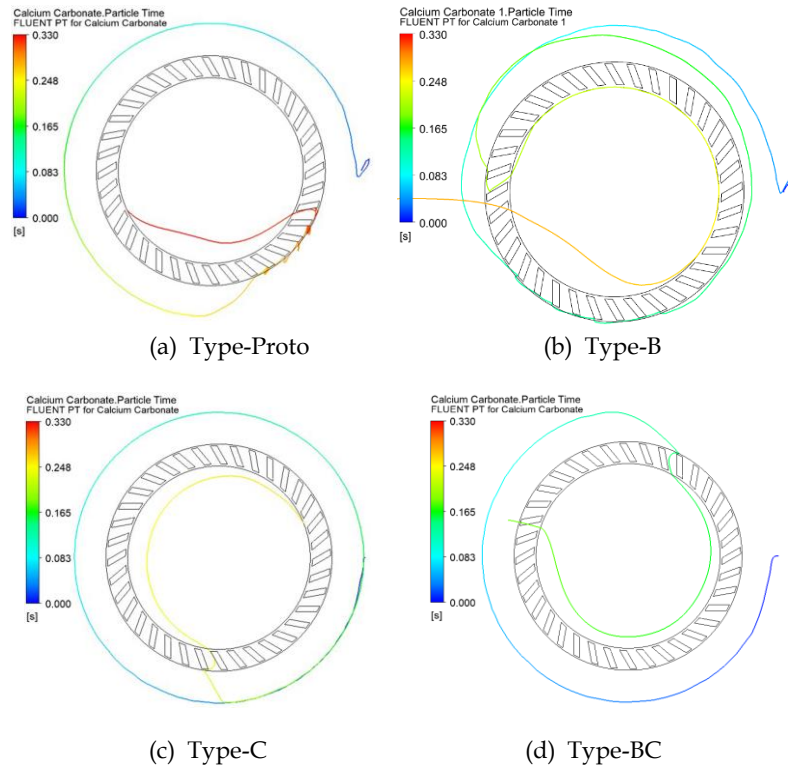


Fig. 11. Comparison of motion trajectories of the particles in the four classifiers

In conclusion, there are two problems with the air inlet layout of Type-Proto. Firstly, the distribution of airflow axial velocity in the elutriation region is not conducive to the transportation of the raw materials; Secondly, the flow field in the rotor cage channels is not well-distributed and there exist obvious vortices. Since Type-B and Type-BC are mirrored and have a position difference of 180° compared with Type-Proto, the maximum positive axial velocity is near the feeding inlet and the raw materials can be carried to the annular region by the upward airflow passing by the elutriation. Type-B and Type-BC have better powder material pneumatic transportation and dispersion capacity compared with Type-Proto and Type-C. Since the airflow forms a clockwise swirling flow after entering the classifier and the rotation direction of the airflow is the same as that of the rotor cage, there are small impact angles of airflow on the blades when the airflow enters the rotor cage, and the flow fields are well-distributed and there exist no vortices in the rotor cage channels for Type-C and Type-BC. It is conducive to the separation of coarse particles and fine particles. Therefore, Type-BC not only enhances the transportation of the raw materials in the elutriation region but also improve the flow field distribution in the rotor cage channels of the classifier. Type-BC is the optimized air inlet layout.

4. Material classification experiments

4.1. Powder raw materials

The calcium carbonate raw materials are prepared through the process of crushing, grinding and sieving of ores, and provided by Lingshou County Yuchuan Mineral Products Co., Ltd, which located in Lingshou County, Shijiazhuang City, Hebei Province, China. The calcium carbonate sample is

analyzed by X-ray Fluorescence Spectrometer (XRF) provided by Beijing University of Chemical Technology. The Analysis report (Oxides of the Elements) show: the proportion of calcium (Ca) element is 95.9957%; the proportion of silica (Si) element is 1.6692%; the proportion of magnesium (Mg) element is 0.9280%; the proportion of Ferrum (Fe) element is 0.5974%; the proportion of aluminum (Al) element is 0.4762%; the proportion of Kalium (K) element is 0.2401%; the proportion of Strontium (Sr) element is 0.0793%; the proportion of phosphorus (P) element is 0.0141%. It means the purity of the calcium carbonate sample is about 96%. Due to the high purity of the sample, to simple the expression, the density of 2700 kg/m³ for calcium carbonate is used as the density of the experimental material in the manuscript. The LT3600 laser particle size analyzer (Chinese Zhuhai Truth Optical Instrument Co., Ltd) is used to measure the particle size of calcium carbonate raw materials and classification products. The particle size differential distribution of calcium carbonate raw material is shown in Table 2.

The morphology of the calcium carbonate sample is also observed and analyzed by Scanning Electron Microscope (SEM) provided by Beijing University of Chemical Technology, shown on Figure 12. According to the observation of microscopic morphology of the calcium carbonate sample, it is found that the ultrafine particles adhere to large particles in the raw material. The powder agglomeration is main reason of fish-hook effect and the bypass value b . The different schemes of air inlet layout will influence the particle's movement and distribution characteristics in the classification flow field of the classifier, which will cause the different particle agglomeration probability and 'fish-hook' effect.

Table 2. Particle size distribution of calcium carbonate sample

Particle size (μm)	Amount of Undersize (%)
<4	14.9
4~15	25.8
15~30	23
30~44	13.6
44~66	14.9
66~87	5.8
>87	2

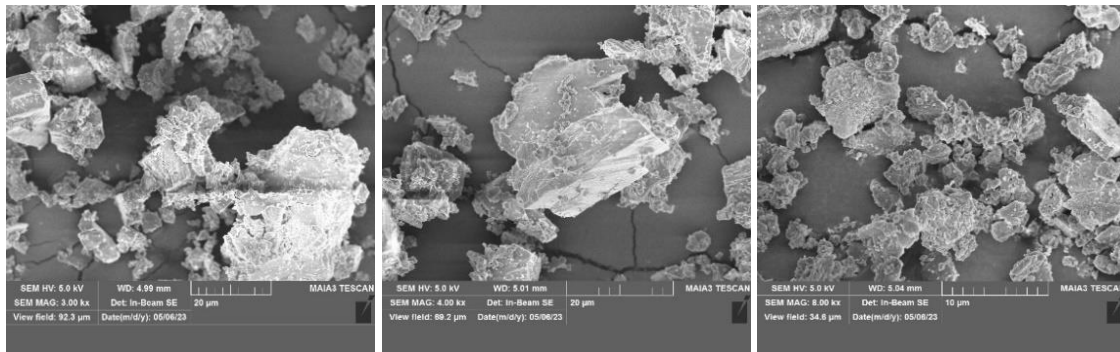


Fig. 12. Microscopic morphology of the calcium carbonate sample observed by SEM

4.1. Classification experiments

Figure 13 shows the pictures of the air intake volute of Type-Proto, Type-B, Type-C, and Type-BC vertical turbo air classifiers. The operating conditions are: feeding speed is 12 kg/h, air inlet velocity is 29 m/s, and rotor cage speed is 800 r/min. The four air inlet layout schemes are used for the classification experiments, respectively. The classification indices of each experiment are calculated, including the cut size d_{50} , the classification accuracy k (d_{25}/d_{75}) and the 'by-pass' value b (Yu et al., 2021). The calculation results are shown in Table 3.

There is a little difference of cut sizes d_{50} among the four schemes and the cut size d_{50} of Type-BC is smallest. The reason is that there is a little difference of the classification force field although their flow

field distributions are different. However, the flow field distribution influences classification accuracy and 'by-pass' value significantly. For Type-B, the classification accuracy k is increased from 48.4% to 53.6% and the 'by-pass' value is decreased from 14.4% to 13.3% compared with Type-Proto. Since Type-B has a stronger elutriation ability, which makes particles fully dispersed and weakens the 'fish-hook' effect, and its classification accuracy is higher, and the 'by-pass' value is lower compared with Type-Proto. For Type-C, the classification accuracy k is increased from 48.4% to 56.4% and the 'by-pass' value is decreased from 14.4% to 11.7% compared to Type-Proto. It can be observed that there exist no vortices in the rotor cage channel of Type-C, therefore the flow field in the channel is well-distributed, which effectively prevents fine particles that have entered the channel from being thrown out of the rotor cage again and back-mixing with coarse particles. As a result, it can improve the classification accuracy and reduce the 'fish-hook' effect. For Type-BC, the classification accuracy k increases by 21.3% from 48.4% to 58.7%, and the 'by-pass' value decreases by 40.1% from 14.4% to 8.5%, compared with Type-Proto. The results demonstrate that the classification performance is significantly improved when the flow fields in the elutriation region and the rotor cage channels are well-distributed at the same time. Type-BC is an optimized scheme of air inlet layout of the classifier.

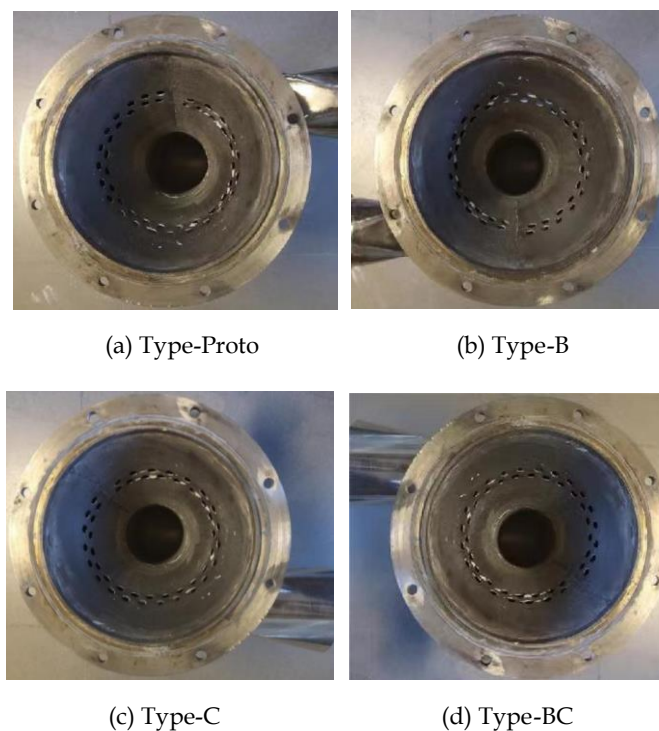


Fig. 13. Pictures of air intake volute with different air inlet layout schemes

Table 3. Experimental results of calcium carbonate powder classification

	Cut size d_{50} (μm)	Classification accuracy k (%)	By-pass value b (%)
Type-Proto	24.1	48.4	14.4
Type-B	23.8	53.6	13.3
Type-C	23.3	56.4	11.7
Type-BC	22.4	58.7	8.5

Conclusions

1. In order to explore the optimization scheme of the air inlet layout of the vertical turbo air classifier, the inner flow field of the vertical turbo air classifier and particle movement trajectory with different air inlet layout schemes are compared and analyzed using the ANSYS numerical simulation software.

2. The numerical simulation results show that the optimization of air inlet layout can effectively improve the flow field distribution in the elutriation region and increase powder material pneumatic transportation and dispersion capacity; the flow field distribution in the rotor cage channel can be improved and the vortex can be eliminated, which will decrease the probability of fine particles back-mixing to the coarse particles. In addition, the particle movement time is shortened and fast classification is completed, which can decrease the particle agglomeration probability.
3. The calcium carbonate classification experimental results indicate that the Type-BC can improve the classification accuracy and weaken the 'fish-hook' effect. Compared with Type-Proto, the cut size is decreased by 7.1% from 24.1 μm to 22.4 μm ; the classification accuracy is increased by 21.3% from 48.4% to 58.7%; the 'by-pass' value is decreased by 40.1% from 14.4% to 8.5%. The Type-BC is the optimal air inlet layout scheme for a vertical turbo air classifier.

Acknowledgments

This project is supported financially by the National Natural Science Foundation of China (No. 52174234).

References

- FENG, L., ZHANG, H., HU, L., ZHANG, Y., WU, Y., WANG, Y., YANG, H., 2020. *Classification performance of model coal mill classifiers with swirling and non-swirling inlets*. Chinese Journal of Chemical Engineering, 28(03), 777-784.
- GAO, Z., WANG, J., LIU, Z., WEI, Y., WANG, J., MAO, Y., 2020. *Effects of different inlet structures on the flow field of cyclone separators*. Powder technology, 372, 519-531.
- GUIZANI, R., MHIRI, H., BOURNOT, P., 2017. *Effects of the geometry of fine powder outlet on pressure drop and separation performances for dynamic separators*. Powder Technology, 314, 599-607.
- HAGEMEIER, T., GLOCKNER, H., ROLOFF, C., THEVENIN, D., JURGEN Tomas., 2014. *Simulation of multi-stage particle classification in a zigzag apparatus*. Chemical engineering & technology, 37(5), 879-887.
- HUANG, Q., LIU, J., YU, Y., 2012. *Turbo air classifier guide vane improvement and inner flow field numerical simulation*. Powder Technology, 226, 10-15.
- KAAS, A., MUTZE, T., PEUKER, U., 2022. *Review on zigzag air classifier*. Processes, 10(4), 764.
- LIM, J., PARK, S., LEE, H., ZAHIR, M., YOOK, S., 2020. *Performance evaluation of a tangential cyclone separator with additional inlets on the cone section*. Powder Technology, 359, 118-125.
- MAGESHWARAN, G., DURAIR., BRITTO, G., JEEVAHAN. J., KURUVILLA, K., FRANCIS, F., 2018, *Computational investigation of flow parameters and efficiency of single and double inlet cyclone separators*. International Journal of Ambient Energy, 39(7), 707-712.
- MAREK, W., LAKHBLR, S., 2019. *Effect of the inlet duct angle on the performance of cyclone separators*. Separation and Purification Technology, 213, 19-33.
- MARTIN, A., TOMAS, S., PECIAR, P., 2017. *Parameters effecting forced vortex formation in blade passageway of dynamic air classifier*. Acta Polytechnica, 57(5), 304-315.
- PETIT, H., IRASSAR, E., 2021. *The throat classifier: A novel air classifier for the control of dust in manufactured sands*. Powder Technology, 390, 417-427.
- REN, C., 2019. *Study on flow field distribution and structure comparison of turbo air classifier*, Beijing: Beijing University of Chemical Technology.
- REN, W., LIU, J., YU, Y., 2016. *Design of Rotor Cage with Arc-blade for the Turbo Air Classifier*. Journal of Mechanical Engineering, 52(2), 195-201.
- REN, W., LIU, J., YU, Y., 2016. *Design of a rotor cage with non-radial arc blades for turbo air classifiers*. Powder Technology, 292, 46-53.
- SU, Y., ZHANG, A., ZHAO, B., 2011. *Numerical simulation of effect of inlet configuration on square cyclone separator performance*. Powder technology, 210(3), 293-303.
- SUN, Z., LIANG, L., LIU, C., ZHU, Y., ZHANG, L., YANG, G., 2021. *CFD simulation and performance optimization of a new horizontal turbo air classifier*. Advanced Powder Technology, 32(04), 977-986.
- SUN, Z., SUN, G., LIU, J., YANG, X., 2017. *CFD simulation and optimization of the flow field in horizontal turbo air classifiers*. Advanced powder technology, 28(6), 1474-1485.
- SUN, Z., SUN, G., LIU, Q., CHAO, J., 2019. *Effects of air inlet type and velocity on classification performance of horizontal turbo air classifier*. Chemical Industry and Engineering Progress, 38 (9), 3956-3961.

- TANG, Z., NIE, B., ZHANG, J., MAN, J., 2013. *Research on the Shape of Blade Side of Vortex Blower*. *Fluid Machinery*, 41(4), 21-25.
- WANG, L., LIU, J., ZHAO, K., YU, Y., 2021. *Influence of a disturbing cone on the flow field and particle classification performance in a vertical turbo air classifier*. *Journal of Beijing University of Chemical Technology (Natural Science)*, 48(6), 87-97.
- WINFIELD, D., CROSS, M., CROFT, N., PADDISON, D., CRAIG, I., 2013. *Performance comparison of a single and triple tangential inlet gas separation cyclone: A CFD Study*. *Powder Technology*, 235, 520-531.
- YU, Y., KONG, X., REN, C., LIU, J., LIU, J., 2021. *Effect of the rotor cage chassis on inner flow field of a turbo air classifier*. *Materialwissenschaft und Werkstofftechnik*, 52, 772-780.
- YU, Y., WANG, L., LIU, J., 2022. *Analysis of numerical simulation models for the turbo air classifier*. *Materialwissenschaft und Werkstofftechnik*, 53(5), 644-657.